Journal of Experimental Botany, Vol. 63, No. 17, pp. 6187–6197, 2012
doi:10.1093/jxb/ers272
This paper is available online free of all access charges (see http://jxb.oxfordjournals.org/open_access.html for further details)

Journal of Experimental Botany
www.jxb.oxfordjournals.org

RESEARCH PAPER

Modulation of plant TPC channels by polyunsaturated fatty acids

Paul Vijay Kanth Gutla[1,*], Anna Boccaccio[1], Alexis De Angeli[2], Franco Gambale[1] and Armando Carpaneto[1,†]

[1] Istituto di Biofisica, Consiglio Nazionale delle Ricerche, Via De Marini 6, 16149 Genova, Italy
[2] Institute of Plant Biology, University of Zurich, Zollikerstrasse 107, CH-8008, Zurich, Switzerland

* Present address: Laboratory of Plant Physiology and Biophysics, Institute of Molecular Cell and Systems Biology, University of Glasgow, G12 8QQ, UK.
† To whom correspondence should be addressed: E-mail: carpaneto@ge.ibf.cnr.it

Received 18 June 2012; Revised 3 September 2012; Accepted 4 September 2012

Abstract

Polyunsaturated fatty acids (PUFAs) are powerful modulators of several animal ion channels. It is shown here that PUFAs strongly affect the activity of the Slow Vacuolar (SV) channel encoded by the plant TPC1 gene. The patch-clamp technique was applied to isolated vacuoles from carrot taproots and *Arabidopsis thaliana* mesophyll cells and arachidonic acid (AA) was chosen as a model molecule for PUFAs. Our study was extended to different PUFAs including the endogenous alpha-linolenic acid (ALA). The addition of micromolar concentrations of AA reversibly inhibited the SV channel decreasing the maximum open probability and shifting the half activation voltage to positive values. Comparing the effects of different PUFAs, it was found that the length of the lipophilic acyl chain, the number of double bonds and the polar head were critical for channel modulation.The experimental data can be reproduced by a simple three-state model, in which PUFAs do not interact directly with the voltage sensors but affect the voltage-independent transition that leads the channel from the open state to the closed configuration. The results indicate that lipids play an important role in co-ordinating ion channel activities similar to what is known from animal cells.

Key words: patch-clamp, plant vacuole, SV channel/TPC1, polyunsaturated fatty acids.

Introduction

Despite the fact that it was discovered in 1987 (Hedrich and Neher, 1987), the physiological role of the Slow Vacuolar (SV) channel is not yet clear (Bonaventure *et al*., 2007*b*; Ranf *et al*., 2008).

The SV current, recorded in all species investigated so far from land (Pottosin and Schonknecht, 2007) to pond water (Paganetto *et al*., 2001) and marine plants (Carpaneto *et al*., 1997), is mediated by a voltage-dependent (Gambale *et al*., 1993), non-selective cation channel (Gradogna *et al*., 2009) that is activated by cytoplasmic calcium (Hedrich and Neher, 1987; Rienmüller *et al*., 2010; Schulze *et al*., 2011). Peiter *et al*. (2005) identified *AtTPC1* as the gene encoding the protein forming the SV channel. AtTPC1 belongs to the family of the so-called two-pore domain channels (Hedrich and Marten, 2011). Among the variety of factors modulating the SV channel, such as magnesium (Pei *et al*., 1999; Carpaneto *et al*., 2001), sodium (Ivashikina and Hedrich, 2005; Perez *et al*., 2008), and reducing agents (Carpaneto *et al*., 1999; Scholz-Starke *et al*., 2004, 2005), the molecular mechanism of regulation of AtTPC1 by vacuolar calcium was recently elucidated (Dadacz-Narloch *et al*., 2011); this was due to the discovery that the point mutation D454N shifted the threshold of activation of TPC1 to more negative voltages with respect to the wild type (Bonaventure *et al*., 2007*b*) and this shift was associated with a reduced sensitivity to vacuolar calcium (Beyhl *et al*., 2009). Interestingly, *Arabidopsis* plants expressing this modified channel, called *fou2* (*fatty acid oxygenation up-regulated 2*)

mutants, present diverse phenotypes such as impaired potassium homeostasis, increased jasmonate levels, and a higher resistance to the pathogen *Botrytis cinerea* (Bonaventure *et al*., 2007*b*). Jasmonates (JA) are plant hormones involved in a variety of processes such as growth, photosynthesis, and plant defence against herbivory (Ballare, 2011). The biosynthesis of JA starts from the polyunsaturated fatty acid (PUFA) α-linolenic acid (ALA, 18:3) that is released from phospholipids by the action of phopholipases A (Browse, 2009).

Despite the fact that PUFAs are well-known and powerful modulators of several voltage-gated ion channels inhibiting or enhancing the activity of calcium, sodium, and potassium channels (Boland and Drzewiecki, 2008), little is known about their effect on ion channels in plant cells. Only one study reported that both arachidonic acid and linolenic acid are modulators of inward and outward ionic currents in the plasma membrane of guard cells (Lee *et al*., 1994).

In this work, the question whether PUFAs influence the activity of ionic currents in plant cells was addressed. The focus was on the major cationic current present in the vacuolar membrane at elevated cytosolic calcium, namely the SV current. First, arachidonic acid (AA) was tested, a widely used PUFA in the animal field, and a strong inhibition of the SV current was found in carrot vacuoles. Then our study was extended to further PUFAs (see Supplementary Fig. S1 at *JXB* online for a list of the fatty acids used in this work) and it was found that, among others, the endogenous linolenic, linoleic, and oleic acids, had similar inhibitory action.

The PUFA's structural requirements for inhibition of the SV current were identified by modifying the polar head, and the length and rigidity of the lipophilic acyl chain.

Materials and methods

Vacuole isolation and patch-clamp measurements

Vacuoles were isolated from carrot taproot parenchyma tissue or from *Arabidopsis thaliana* mesophyll protoplasts (Col-0 wild type). Details on plant culture, vacuole isolation and patch-clamp recordings are described elsewhere (Scholz-Starke *et al*., 2004, 2006). Patch-clamp experiments were performed in excised-patch configuration with the cytosolic side exposed to the bath. Standard bath cytosolic solution was (in mM): 100 KCl, 1 $CaCl_2$, 10 HEPES, 1 DTT, pH 7.5 (with TRISs). Standard pipette vacuolar solution contained (in mM): 200 KCl, 10 MES, pH 5.5 (with TRIS). In both solutions D-sorbitol was added up to 600 mOsm. Data from Figs 1 and 2 were recorded in standard ionic solutions containing 2 mM $MgCl_2$ in both the bath and pipette.

Fatty acids and methyl esters were dissolved at a concentration of 100 mM in 99.5% ethanol. They were stored at –20 °C and diluted in control solution at the desired concentration just before use. Preparation and handling of fatty acids and methyl esters were done in glass reservoirs and capillaries to avoid adsorption processes. All chemicals were purchased from Sigma.

A Perspex recording chamber was designed to allow a delicate and fast change of the bath solution (1 ml min^{-1}; complete exchange of solution in less than 30 s). Ionic solutions containing PUFAs were sucked in glass capillaries (1 mm diameter) connected to oil-filled syringes controlled by a stepping motor and the flow was regulated at a rate of 50 µl min^{-1}. The capillary was then moved in the recording chamber and the tip of the patch pipette was placed inside the opening. This experimental design assured a good control of the PUFA concentration. For wash out, the glass pipette was removed and the excised patch was washed with fresh solution.

Data analysis

The polarity of current and voltage follow the convention proposed by Bertl *et al*. (1992). Positive currents represent positive charge going from the cytosol to the vacuolar lumen.

Normalized conductance was calculated from instantaneous tail currents at the potential of –50 mV. The tail current was fitted with a single exponential function and the value at the beginning of the tail voltage step, corrected for a filter delay of 0.3 ms, was extrapolated. The fit was performed about 1 ms after the onset of the tail voltage in order to remove the capacitance artefact. For a single vacuole, data in the control were fitted with a Boltzmann equation; then both control and AA data were normalized to the maximum of the Boltzmann in control condition, indicated as G_{norm}, and data from different vacuoles were averaged.

The dose–response of AA inhibition at each potential was obtained by plotting the normalized conductance (G_{norm}) versus AA concentration. To fit the dependence of the residual current on the AA concentration, the Hill function $G_{norm}=G_{max}/(1+([AA]/K_h)^n)$ was used, where $[AA]$ is the AA concentration, K_h and n are the Hill half-inhibition constant and the Hill coefficient, respectively.

For non-stationary noise analysis, the mean current and variance were calculated using 50 consecutive sweeps; the time interval between two consecutive sweeps was 2 s and the voltage and duration of the single sweep were –50 mV and 0.1 s, respectively. Every single sweep was preceded by a voltage pulse of +80 mV lasting 0.5 s. The holding voltage was –50 mV. To partially eliminate linear drifts usually present in patch-clamp recordings, the variance was calculated using the difference of all pairs of consecutive sweeps, as suggested by Heinemann and Conti (1992).

Data are presented as mean ±standard error, with n indicating the number of experiments. Statistical significance was determined using unpaired t tests, or ANOVA. Unless otherwise stated, the statistically significant difference was determined with ANOVA and a Tukey *post hoc* test was done to evaluate which data groups showed significant differences. P values <0.05 were considered significant, <0.01 highly significant.

Data analysis, figures and simulations were made with Igor software (Wavemetrics, Lake Oswego, OR, USA).

Results

Arachidonic acid reversibly inhibits the Slow Vacuolar current in carrot root vacuoles

Macroscopic Slow Vacuolar (SV) currents were recorded in excised cytosolic side-out patches from vacuoles isolated from carrot roots. The outward rectifying currents were elicited by a series of voltage steps ranging from –80 to +120 mV in +10 mV steps, from a holding potential of –50 mV. Currents were inhibited by 10 µM AA, as shown in Fig. 1A. The inhibition was fully reversible and concentration-dependent. Figure 1B shows the normalized conductances with respect to the maximum measured in control conditions, G_{norm} (see also the Materials and methods), obtained from instantaneous tail currents and plotted as a function of the activating potential for different AA concentrations (1, 3, and 10 µM). Experimental data are well-described by a Boltzmann function (continuous lines) with parameters obtained from a simple three-state model (see below and the Appendix in the Supplementary data at *JXB* online): AA decreased the maximum value of the normalized conductance and shifted the half-activation voltage to more positive values. The dose dependence of AA inhibition of the SV current was analysed at different potentials by plotting G_{norm} as a function of AA concentration. The inset in Fig. 1C shows a plot of G_{norm} versus the AA

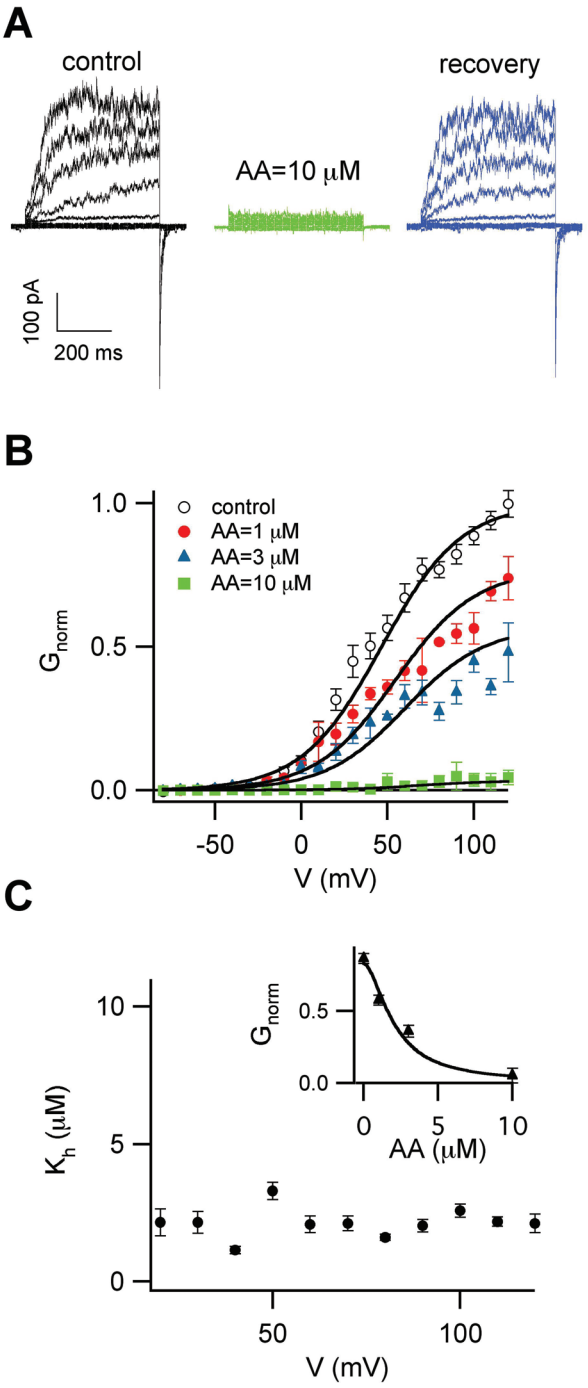

Fig. 1. Arachidonic acid reversibly inhibits the Slow Vacuolar current in excised patches from carrot root vacuoles. (A) Macroscopic SV currents elicited by a series of voltage steps ranging from –80 to +120 mV in +10 mV steps and recorded from a carrot root vacuole in control conditions, in the presence of arachidonic acid (10 μM AA) and after washout (recovery). For the sake of clarity, only traces from –80 to +100 in +20 mV step were shown. The holding potential was –50 mV. (B, C) Quantitative analysis of SV current inhibition by arachidonic acid. (B) Normalized instantaneous tail currents, G_{norm}, plotted as a function of the activating potential for different AA concentrations, 0 (n=5 experiments from independent vacuoles), 1 (3), 3 (3), and 10 μM (3). Continuous lines represent the Boltzmann equation: $G_{norm}=G_{max}/(1+\exp(-(V-V_h)/s))$. Data were normalized to 1 in the absence of AA ($G_{max}(0)=1$); the other parameters, obtained by application of a three-state model to both stationary and non-stationary data (see Appendix in the Supplementary data at *JXB* online), were (in parentheses we indicate the concentration of AA in μM): $V_h(0)$=47 mV, $G_{max}(1)$=0.77, $V_h(1)$=55 mV, $G_{max}(3)$=0.57, $V_h(3)$=60 mV, $G_{max}(10)$=0.03, $V_h(10)$=70 mV. The slope factor (s) was 23 mV. (C) The inset shows an example of G_{norm} at a test potential of +90 mV plotted as a function of AA concentration. The continuous line represents the fit with a Hill equation, with half inhibition constant K_h(+90 mV)=2.0±0.2 μM. The Hill coefficient n=1.8±0.1 was obtained by a global fit of the data at all voltages. In the main panel, K_h values are plotted against the applied membrane voltages. (This figure is available in colour at *JXB* online.)

concentration at +90 mV and fitted with a Hill equation (continuous line). K_h values, derived as for the example potential in the inset, were plotted versus the applied membrane voltage in the main panel of Fig. 1C. The Hill coefficient n=1.8±0.1, obtained by a global fit of the data at all voltages, indicated that more than one fatty acid molecule interacted with the channel. K_h did not show any pronounced voltage dependence.

AA also affects the SV channel kinetics. Indeed, both activation and deactivation time courses were accelerated as shown on an expanded time-scale in the insets of Fig. 2A. To quantify the effect of AA on the activation kinetics, the time required for half activation (t_{half}) versus the applied membrane voltage in control conditions and 1 μM and 3 μM AA was plotted, as shown in Fig. 2B. The deactivation of the SV current could be fitted with a single exponential function and the resulting time constant, τ, is shown in Fig. 2C (continuous lines in the upper right inset of Fig. 2A represent the exponential fit of the tail current). This analysis showed that the effect of AA on deactivation is more pronounced than on activation kinetics.

Arachidonic acid does not affect single channel properties but decreases the maximum open probability

The analysis of macroscopic currents showed a marked decrease of maximum normalized conductance, G_{norm}, upon AA application, which may depend on a modification of channel conductance, number of channels, and maximal open probability or on a combination of these three factors.

It was first checked whether AA modified the SV single channel conductance. Single channels events could be measured during the deactivation of the macroscopic current at a tail potential of –50 mV, as shown in Fig. 3A. Current step amplitude was not modified by the presence of 3 μM AA, while the duration of single events was much shorter, consistent with the faster deactivation time course reported in Fig. 2A and 2C.

Single channel current–voltage relationships were obtained from the application of a fast voltage-ramp (3 V s^{-1}) during the deactivation process (Pottosin *et al*., 2001; Scholz-Starke *et al*.,

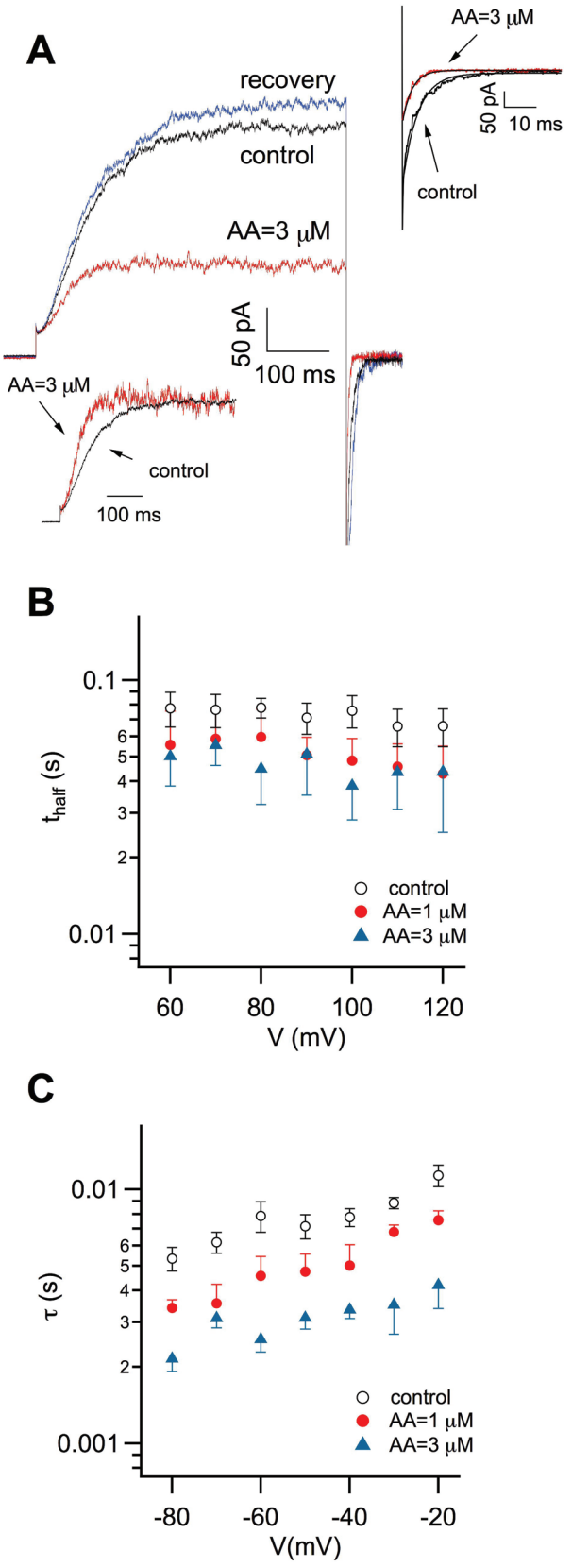

Fig. 2. Arachidonic acid accelerates both activation and deactivation time course of Slow Vacuolar currents. (A) Macroscopic SV currents recorded at a voltage step of +80 mV in control conditions, in the presence of arachidonic acid (3 μM AA) and after washout (recovery). The holding potential was –50 mV. The insets show that both the activation (bottom inset) and the deactivation time-course (right side inset) are faster in the presence of AA. The time required for half-activation was 74.3 ms in the control and 47.9 ms in 3 μM AA. The tail voltage was of –40 mV. The deactivating current could be fitted with a single exponential, shown on the right side inset as continuous lines (with a τ of 6.3 and 2.8 ms, respectively, in the control and in 3 μM AA). (B) The time required for half-activation of the current (t_{half}) is plotted against the applied membrane potential in control (open circles; n=5) and in the presence of 1 μM (closed circles; n=3) or 3 μM (filled triangles; n=3) AA. (C) Time constants of current deactivation, τ, in control (open circles; n=5) and in the presence of 1 μM (closed circles; n=3) or 3 μM (filled triangles; n=3) AA are plotted against the tail potential. (This figure is available in colour at *JXB* online.)

2004). If the ramp is sufficiently fast, it is possible to span the entire current–voltage characteristic of one single channel from –50 mV up to +100 mV before more events superimpose. The protocol was repeated several times and baseline traces without channel openings were subtracted from traces containing a single opening. Single channel current–voltage relationships obtained with this procedure are shown in Fig. 3B and strongly suggest that the single channel conductance does not change in the presence of AA in the whole range of investigated voltages.

The smaller single channel conductance at positive voltages with respect to negative voltages is due to the working conditions, i.e. low cytosolic (100 mM) and high vacuolar (200 mM) potassium concentrations, together with the presence of high cytosolic calcium (1 mM), which, competing with potassium, can reduce the single channel current at positive voltages. The arrow in Fig. 3B indicates the Nernst equilibrium voltage of potassium (15.9 mV), which is in agreement with a high selectivity of K^+ through SV channels in these experimental conditions (for a detailed discussion of calcium/potassium selectivity/permeability see Allen *et al*., 1998; Gradogna *et al*., 2009). Since the single channel conductance was not affected by AA, the significant reduction of G_{max} shown in Fig. 1B could be due to a decrease in the total number of channels (N) present in the patch and/or a decrease in maximum open probability (P_{Omax}). To discriminate between these two possibilities non-stationary noise analysis was performed. The variance of the current was calculated (Heinemann and Conti, 1992; see also Materials and methods) and it was plotted against the mean of the deactivating current at –50 mV for the same patch in the control and in the presence of 3 μM AA as shown in Fig. 3C. The solid curve in Fig. 3C is the fit of the control data using the parabolic function $\sigma^2=iI-I^2/N$, where σ^2 is the variance, i the single channel current at –50 mV, I the mean current, and N the total number of channels, yielding N=42 channels and i=12 pA in the control (empty circles). Data in the presence of AA (filled circles) are not significantly displaced from control data, excluding a reduction of N due to AA action and pointing to a decrease in maximum open probability. Data points at low current amplitudes, corresponding to low open probabilities, can be fitted with a line whose slope is the single channels current, i; the overlap between data points in

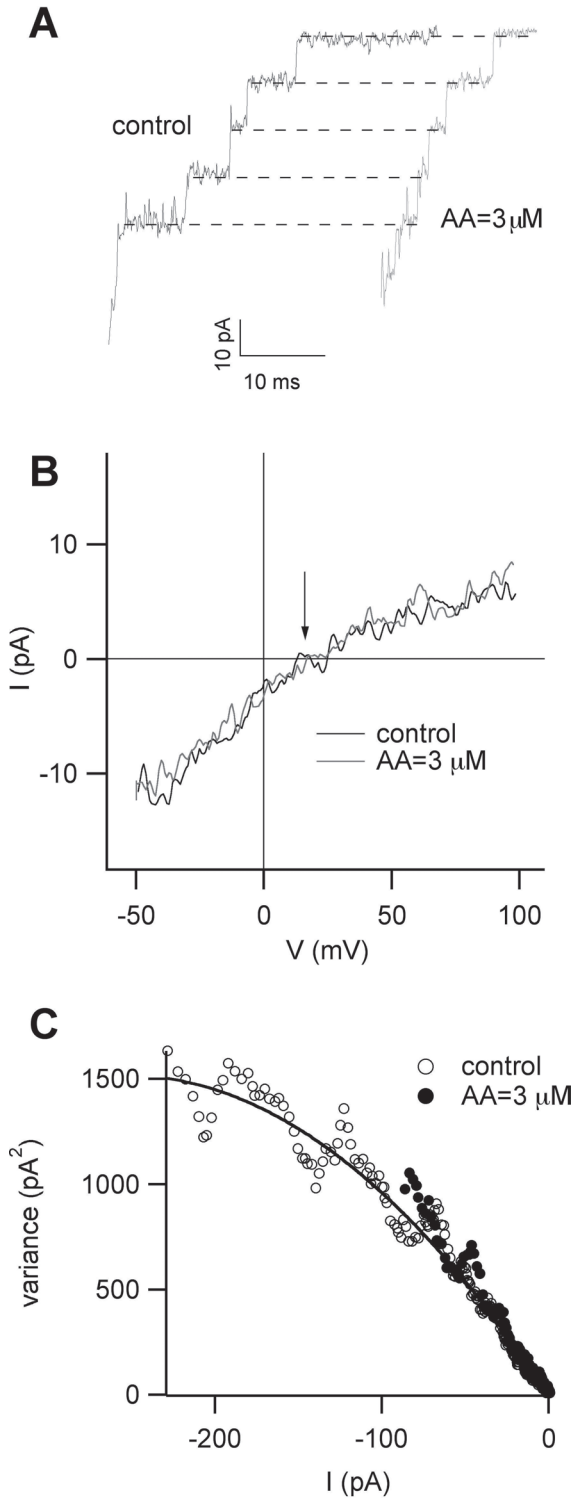

Fig. 3. Arachidonic acid does not change single channel conductance of Slow Vacuolar current in carrot roots but affects its maximum open probability. (A) Single channel events obtained during deactivation at a tail voltage of –50 mV in control conditions (black trace) and in 3 μM AA (grey trace). (B) Single channel current–voltage relationships obtained after the application of a fast voltage-ramp in control conditions (black trace) and in 3 μM AA (grey trace). No change in single channel conductance was apparent. The slope conductances at negative and positive voltages were 160 ± 12 pS and 54 ± 7 pS, respectively. (C) Non stationary noise analysis for the same patch in control (empty circles) and in presence of 3 μM AA (filled circles) at the potential of –50 mV. Variance is plotted against the mean current and the solid curve is the fit to the control data with a parabolic function (see text and Materials and methods). Data in the presence of AA are not significantly displaced from control data, excluding an effect of AA on single channel conductance and a reduction in the total number of channels.

control and 3 μM AA confirms that the single channel current is not affected by AA, as already shown in Fig. 3A and 3B.

Modulation of Slow Vacuolar current depends on PUFAs structural properties

From a chemical point of view, PUFAs are formed by a hydrophobic fatty acyl tail and a carboxylic polar head which are both important for the modulation of ionic channels (Borjesson *et al*., 2008). The effects of the length of the acyl tails on the PUFA inhibition of the SV current was investigated. Twenty-two and 18 carbon long PUFAs were used as well as docosahexaenoic acid (DHA) and alfa-linolenic acid (ALA) that have a longer and a shorter tail lengths compared with AA (20 carbons).

Figure 4A shows the reversible inhibition of the SV currents induced by 3 μM and 10 μM DHA and ALA compared with AA. DHA and AA had a similar efficacy, while ALA was less efficient in inhibiting the SV current both at 3 μM and 10 μM (P <0.01), as summarized in the histogram in Fig. 4B. As observed for AA, DHA and ALA also modify the current kinetics in a similar manner, as shown in Table 1. The effect of PUFAs on isolated vacuoles of mesophyll cells from the model plant *Arabidopsis thaliana* was also tested. At +80 mV, $I_{PUFA}/I_{control}$ was 0.64 ± 0.07 for 10 μM ALA (four repetitions in two different vacuoles) and 0.40 ± 0.05 for 10 μM AA (six different vacuoles), with AA significantly more effective than ALA (unpaired t test, P <0.05). These data demontrate that PUFAs are also strong inhibitors of the *Arabidopsis* TPC1 channel (see alsoTable 1).

The number of double bonds in the acyl tail of PUFAs affects the tail flexibility and therefore may affect the insertion of the PUFA in the membrane and its motility. Therefore, the effect of PUFAs with the same number of carbons, but with a variable number of double bonds (Fig. 5A, 5B) was investigated in isolated vacuoles of carrot roots: linolenic acid, ALA (C18:3) with three double bonds, linoleic acid LA (C18:2) with two double bonds, and oleic acid OA (C18:1) with a single double bond. Since stearic acid (C18:0) was not soluble in our conditions, other saturated PUFAs with shorter (palmitic acid, PA, 16 carbons) and longer chain lengths (arachidic acid, ARA, 20 carbons) were tested. Figure 5A shows the current traces in the control and in the presence of 100 μM of different PUFAs, except for ARA which was used at 10 μM due to its limited solubility in our experimental conditions. However, it is worth comparing ARA with AA at 10 μM (see Fig. 4 which has the same number of carbons at the tail but four double bonds). The efficacy of ALA, LA, and OA is very similar at 10 μM and 30 μM as summarized in the histogram in Fig. 5B. OA at 100 μM is less effective than ALA and LA (P <0.01), while the saturated PUFAs, PA and ARA, did

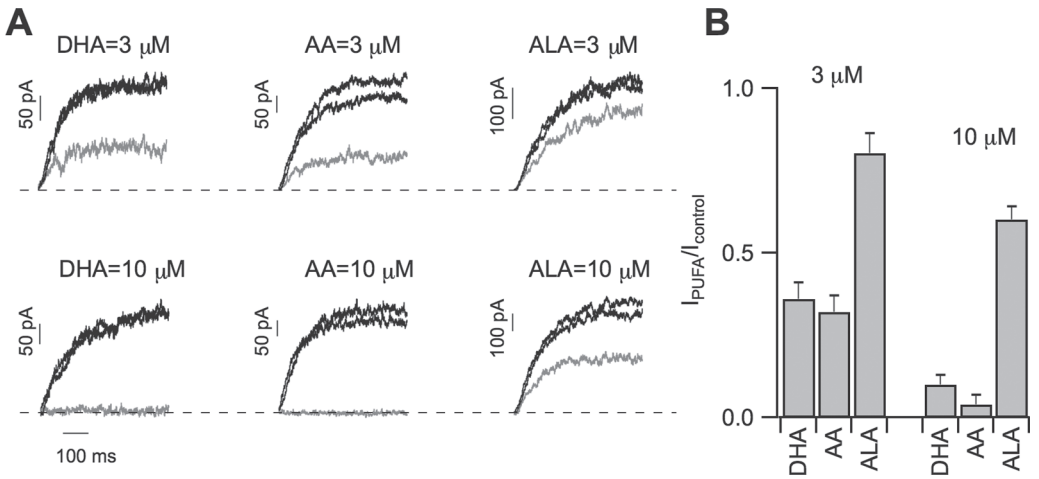

Fig. 4. Modulation of Slow Vacuolar current by different PUFAs. (A) Macroscopic SV currents recorded at a voltage step of +80 mV in control conditions and after washout (black traces), in the presence of either DHA (C22), AA (C20) or ALA (C18) at 3 μM (upper panels, grey traces) or 10 μM (lower panels, grey traces) and after washout (recovery, blue). (B) Residual SV currents ($I_{PUFA}/I_{control}$) obtained by dividing the current in the presence of PUFA at the indicated concentration by the current in control conditions for DHA (n=7), AA (10), and ALA (10) at 3 μM and for DHA (4), AA (7), and ALA (10) at 10 μM. DHA and AA had a similar efficacy while ALA was less efficient both at 3 μM and 10 μM (P <0.01). (This figure is available in colour at *JXB* online.)

Table 1. Kinetics of SV currents in isolated vacuoles from carrot and Arabidopsis. Activation and deactivation kinetics are quantified, respectively, with the time required for half activation (t_{half}) and the time constant of the exponential fit, τ.

	$t_{halfPUFA}/t_{halfcontrol}$ [a]	$\tau_{PUFA}/\tau_{control}$ [a]	Number of vacuoles
Carrot			
DHA 3 μM	0.84 ± 0.09	0.42 ± 0.07**	7
AA 3 μM	0.83 ± 0.06*	0.44 ± 0.07**	10
ALA 10 μM	1.07 ± 0.05	0.53 ± 0.06**	10
LA 10 μM	0.76 ± 0.07*	0.39 ± 0.03**	4
OA 10 μM	0.67 ± 0.07*	0.51 ± 0.16	4
Arabidopsis			
AA 10 μM	1.05 ± 0.18	0.27 ± 0.08**	6
ALA 10 μM	1.34 ± 0.09	0.50 ± 0.06	2 (4)

[a] Asterisks (*) and (**) indicate, respectively, significant and highly significant statistical difference (*t* test). Data with ALA 10 μM in Arabidopsis were not tested for statistical significance; the number in parenthesis indicates the number of repetitions.

not change the current significantly. Our data suggest that the bending of the hydrophobic chain of the fatty acids, that requires at least a double bond (see Supplementary Fig. S2 at *JXB* online), is important for PUFA's inhibition of TPC channel.

Figure 5C shows the time-course of the stationary current recorded at +80 mV upon application and removal of ALA and OA at 30 μM; maximal and minimal currents obtained, respectively, in the absence and in the presence of PUFAs were set to 1 and 0, respectively, and the other values were scaled accordingly. ALA at 30 μM inhibited the SV current in about 20 s, comparable with the time necessary to exchange the solution, while in identical working conditions, a longer time was required for the inhibition of OA and for recovery. Since OA is supposed to partition in the membrane phase with high efficiency (Simard *et al.*, 2008), we can speculate that this result is in line with a direct interaction between PUFAs and the channel (see Discussion).

In Fig. 6, the role of the negative charge present at the polar head of the PUFAs was investigated. The SV current was challenged with neutral methyl esters of the PUFAs. Figure 6A shows that both Me-ALA and Me-DHA were, respectively, ineffective or slightly effective (P <0.01) in inhibiting the SV current at a concentration of 100 μM, while inhibition was complete when ALA was applied at the same concentration and DHA at 10 μM (Fig. 4A). Thus the negative charge of the polar head of the PUFAs is an essential structural characteristic for the modulation of SV current.

Modelling the PUFA effect

We propose a very simple model that can predict all our experimental findings. The kinetic scheme is the following: scheme 1

$$C_0 \underset{\beta(V)}{\overset{\alpha(V)}{\rightleftarrows}} C_1 \underset{k_C([PUFA])}{\overset{k_o}{\rightleftarrows}} O$$

According to this model the channel can be in three states: C_0 and C_1 are the closed states and O is the conductive open

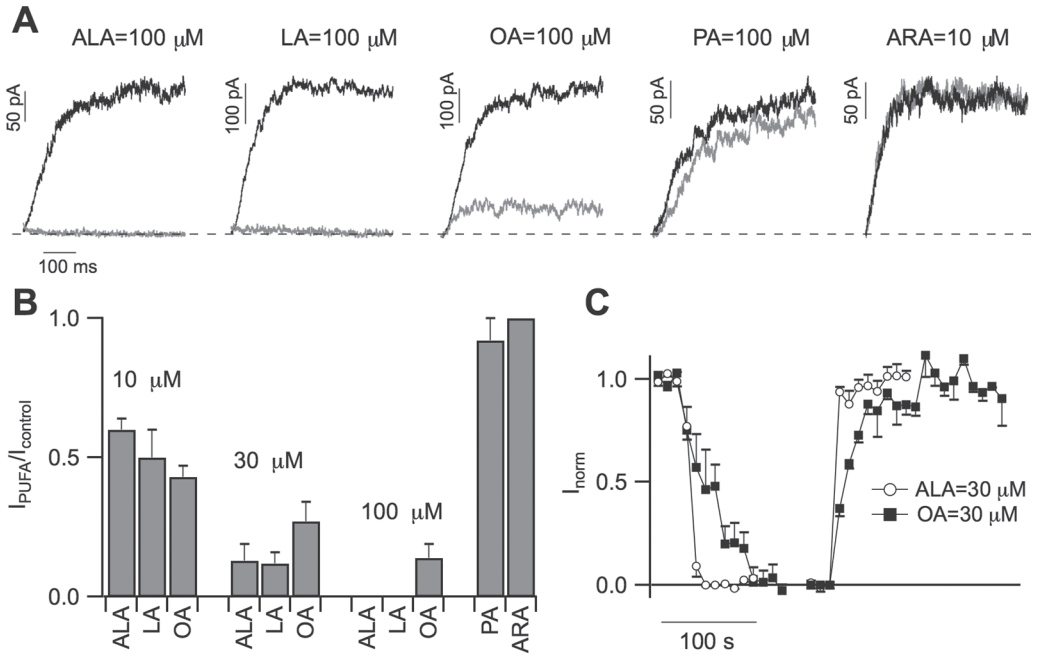

Fig. 5. Modulation of Slow Vacuolar current depends on the degree of fatty acid saturation. (A) SV currents recorded at +80 mV in control conditions (black traces), in the presence of either ALA (3 double bonds), LA (2 double bonds), OA (1 double bond), PA (no double bond), and ARA (no double bond) at 100 μM, except ARA at 10 μM (grey traces). (B) Residual SV currents at +80 mV normalized to control ($I_{PUFA}/I_{control}$) for 10, 30, and 100 μM ALA (*n*=10, 3, and 4 different vacuoles), LA (*n*=4, 4, 3), and OA (*n*=4, 4, 3). PA (*n*=3) and ARA (*n*=4) were little or not effective, respectively, at 100 μM and 10 μM. The efficacy of ALA, LA, and OA was not significantly different at 10 μM and 30 μM, while OA at 100 μM was less effective than ALA and LA (P <0.01). (C) Time-course of the inhibition and recovery induced by 30 μM ALA (filled circles, *n*=3) and OA (filled squares, *n*=3). The average maximum and minimum values of the stationary currents recorded at +80 mV in the absence and in the presence of PUFAs were set to 1 and 0, respectively, and the other values scaled accordingly.

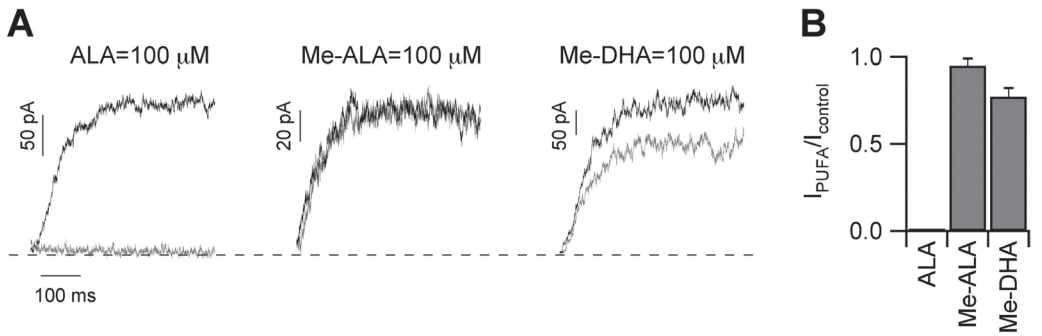

Fig. 6. Modulation of Slow Vacuolar current depends on the polar head of the PUFA. (A) Macroscopic SV currents elicited by a voltage step of +80 mV in control conditions (black traces) and in the presence of either ALA, Me-ALA, or Me-DHA at 100 μM (grey traces). (B) Residual SV currents at +80 mV normalized to controls ($I_{PUFA}/I_{control}$) for ALA (*n*=4), Me-ALA (*n*=3), and Me-DHA (*n*=3) at 100 μM. Me-ALA and Me-DHA were, respectively, ineffective or only slightly effective (P <0.01).

state. The first step from C_0 and C_1 is voltage dependent and represents the movement of the four voltage sensors S4 due to the application of an electric field. For the sake of simplicity, the transition of the four S4 are grouped in a single step in which the rate constants α and β are voltage dependent. The step from C_1 to O leading to the opening of the channel is assumed to be voltage-independent, therefore k_O and k_C are voltage-independent rate constants (Schmidt and MacKinnon, 2008; Borjesson and Elinder, 2011). It is worth noting that only k_C, leading the channel from the open state O to the closed state C_1, is PUFA-dependent. The analytical resolution of the model is given in the Appendix of the Supplementary data at *JX*B online. The simulation of the experimental data by the model is presented in Fig. 7.

Both stationary data of Fig. 7A and the relaxation time constants of Fig. 7B are adequately described by the model as shown by the satisfactory overlap of the continuous theoretical lines and the experimental data points (for details see the Appendix section 'Simulation of the model' in the Supplementary data at

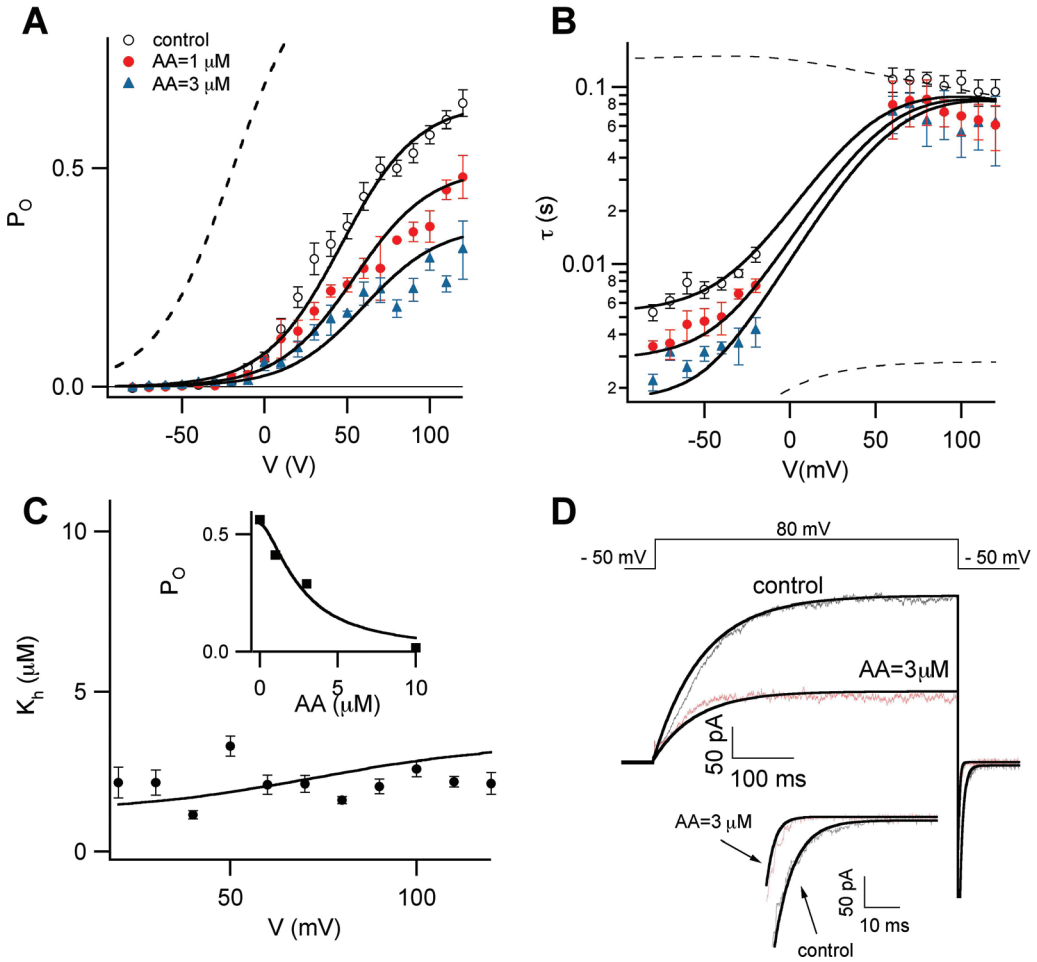

Fig. 7. The three state model: simulation of the PUFA effect and comparison with experimental results. (A) Open probability and (B) time constants of relaxations of the SV channels in the absence (open circles) and in the presence of 1 μM (closed circles) and 3 μM (closed triangles) AA versus applied potential. The continuous lines were obtained, respectively, using equations A.4 and A.14 (see the Appendix in the Supplementary data at *JXB* online for details). Dashed lines correspond to k_C=7. (C) In the inset, the stationary open probability at +90 mV was obtained by equation A.4 versus AA concentration (see the Appendix in the Supplementary data at *JXB* online for details). The continuous line is the fit of the data points with the Hill equation: $K/(1+([AA]/K_h)^n)$, where K is a normalization factor. This operation was repeated for all voltages from +20 to +120 mV at a step of +0.5 mV. The average Hill coefficient n was 1.6±0.2. In the main panel, K_h values were plotted versus the applied membrane voltage (black line) and overlapped to the same data points of Fig. 1C. (D) Overlapping between experimental and theoretical currents in the absence and presence of 3 μM AA. The imposed voltage protocol is shown in the upper part of the figure. The theoretical currents were obtained by equation A.16 (see the Appendix in the Supplementary data at *JXB* online for details). (This figure is available in colour at *JXB* online.)

JXB online). The model has six independent parameters; however, the variation of only k_C, is sufficient to predict both stationary and transient data in the presence of PUFA. An increase of k_C generates the traces in the presence of increasing concentrations of AA; by contrast, the dotted traces in Fig. 7A and 7B are obtained with decreasing k_C up to 7 s^{-1} that provides a Boltzmann curve with a voltage of half activation of –20 mV and a maximum open probability near 1. Therefore, our model shows a shift of the voltage-dependency of the SV channel toward physiological voltages upon reduction of k_C. To analyse the dose dependence of PUFA inhibition theoretical P_O versus AA concentration at a fixed voltage was plotted, as shown in the inset of Fig. 7C (V= +90 mV). Data were fitted by the Hill equation; the continuous line in the inset and K_h values were plotted against the potential as shown by the continuous line of Fig. 7C; points in the same figure represent K_h obtained from experimental data (already plotted in Fig. 1C). In agreement with experimental findings, K_h derived by the model does not show a pronounced voltage dependence reflecting the fact that the binding of PUFAs with the channel is actually voltage independent. In Fig. 7D, experimental traces in the absence (grey traces) and in the presence of 3 μM AA (red traces) were well reproduced by our model (black traces); small differences in activation between data and theory were due to the simplifying hypothesis of a single voltage dependent step. In the deactivation process, the agreement was very good as shown by the inset. There is a need to emphasize that the simulation of the experimental data in the presence of AA was obtained with the same parameters used to reproduce control data, except k_c, the voltage-independent rate of deactivation.

Discussion

How do PUFAs interact with the TPC channels? PUFAs have the ability to form micelles that, by fusing with the lipid bilayer, can affect cell membrane organization and alter channel function. However, the concentration range used in this study is low enough to exclude this possibility (Linden and Routtenberg, 1989; Borjesson *et al*., 2008), hence fatty acids should act as monomers. The following lines of evidence suggest that the interaction between PUFA and the channel is direct and not mediated by a modification on the vacuolar membrane due to PUFA incorporation. PUFAs are known to increase membrane fluidity (Anel *et al*., 1993), however, in this case, a similar effect should be obtained by the application of the methyl-ester forms of PUFAs, which in our case were either ineffective (Me-ALA, Fig. 6) or only slightly effective (Me-DHA, Fig. 6). In addition, the time-course of application of OA was slower compared with the other PUFAs even though the partition coefficient of OA in the membrane phase is comparable (Anel *et al*., 1993; Simard *et al*., 2008), again in contrast with an effect of PUFA on membrane fluidity. PUFAs are known to modify the membrane curvature, but in this case the effect of DHA is expected to be greater than the effect of AA, as shown for TRAAK channels (Patel *et al*., 2001). On the contrary, our data show that the inhibition of SV by PUFAs is maximal when the channel is exposed to AA (Fig. 4). Indeed, the finding of an optimal length of the acyl chain/number of double bonds of the PUFA is clearly not indicative of an unspecific change of the membrane properties.

Another well-known effect of PUFAs on biological membranes is the screening of surface charges (Borjesson *et al*., 2008) resulting in a shift of the voltage-dependence of the channel. However, charge screening cannot induce a reduction of the maximal open probability, which was observed in our data. The kinetic properties of the channel are also in contrast with that mechanism: a faster time-course of deactivation at negative voltages would correspond to a slower time-course of channel activation at positive voltages. Nevertheless, the charge of the PUFA head seems to play an important role in channel inhibition, since neutralization largely reduced or eliminated the inhibitory effect. As suggested by the voltage-independent apparent binding constant of PUFA, we can hypothesize that the interaction between the PUFA head and the channel is very likely of electrostatic nature, but located outside the electric field. The hydrophobic moiety appears to be an important factor for the PUFAs' efficacy. The higher the number of cis double bonds in the PUFA, the more hooked will be its conformation. Notably, the bending of the hydrophobic tail correlates well with the inhibitory power, with the curved ones being the most potent (see Supplementary Fig. S2 at *JXB* online). This observation suggests that the interaction between the PUFA and the channel and the efficacy of the inhibition depend on the specific geometry of the PUFA.

An important finding of our work is that free PUFAs can interact with and modulate the activity of TPC1. In the present study, it was found that the most effective PUFA in inhibiting the SV current is arachidonic acid, effective at low micromolar concentrations, in the physiological range reported for animal cells (Meves, 1994, 2008). Although plant do not synthesize this fatty acid (Singh *et al*., 2005), it has been shown that some pathogens, such as *Phytophthora infestans*, harbour arachidonic acid in their membranes and that this molecule is an elicitor of plant defence responses (Yoshioka *et al*., 2001). However, it is unlikely that an elicitor of the pathogen defence response acts directly on a vacuolar ion channel.

One of the most important endogenous PUFAs is alpha-linolenic acid (ALA) which, in our experiments, was found to inhibit the SV/TPC1 currents when applied in the micromolar range (Fig. 4). ALA is the most abundant fatty acid in leaves and mostly present in esterified glycerolipid form (Browse and Somerville, 1991). From data in the literature (see Supplementary Table S1 at *JXB* online), a basal ALA concentration can be estimated of about 1 μM increasing up to 10 μM during physiological processes such as pathogen elicitation and wounding. According to our data, such an increase in ALA concentration should significantly inhibit the activity of the TPC1 channel, therefore making it unlikely that the channel plays an active role in the plant response to these kinds of stresses. In agreement with this hypothesis, experiments performed in tpc1-2 knock-out plants showed no significant involvement of TPC1 in the jasmonate pathway (Bonaventure *et al*., 2007*a*).

In conclusion, it is shown that the activity of the SV/TPC1 channel is strongly affected by polyunsaturated fatty acids in vacuoles of carrot roots and in *Arabidopsis thaliana*. Since the modulation of membrane proteins by lipids is a poorly explored topic in plants we think that our data open new perspectives in the field of ion channels and lipid-mediated interaction in plants.

Supplementary data

Supplementary data can be found at *JXB* online.

Supplementary Fig. 1. List of fatty acids used in this study.

Supplementary Fig. 2. Three-dimensional conformation of the different fatty acids used in the experiments.

Supplementary Table S1. Free fatty acids(FFA) in different plant preparations in control conditions and after different treatments.

Acknowledgements

We thank Joachim Scholz-Starke and Oscar Moran (Istituto di Biofisica, CNR, Italy) for useful discussions. We acknowledge Joachim Scholz-Starke for critical comments on the manuscript. Mathematical support for the model part by Paolo Lorenzoni (University of Milano Bicocca) was highly appreciated. We acknowledge the financial support by the EU Research Training Network 'VaTEP' (CT-2006–035833) and by 'Progetti di Ricerca Nazionale' (bando 2008).

References

Allen GJ, Sanders D, Gradmann D. 1998. Calcium–potassium selectivity: kinetic analysis of current–voltage relationships of the open, slowly activating channel in the vacuolar membrane of *Vicia faba* guard-cells. *Planta* **204,** 528–541.

Anel A, Richieri GV, Kleinfeld AM. 1993. Membrane partition of fatty acids and inhibition of T cell function. *Biochemistry* **32,** 530–536.

Ballare CL. 2011. Jasmonate-induced defenses: a tale of intelligence, collaborators and rascals. *Trends in Plant Science* **16,** 249–257.

Bertl A, Blumwald E, Coronado R, *et al.* 1992. Electrical measurements on endomembranes. *Science* **258,** 873–874.

Beyhl D, Hortensteiner S, Martinoia E, Farmer EE, Fromm J, Marten I, Hedrich R. 2009. The fou2 mutation in the major vacuolar cation channel TPC1 confers tolerance to inhibitory luminal calcium. *The Plant Journal* **58,** 715–723.

Boland LM, Drzewiecki MM. 2008. Polyunsaturated fatty acid modulation of voltage-gated ion channels. *Cell Biochemistry and Biophysics* **52,** 59–84.

Bonaventure G, Gfeller A, Proebsting WM, Hortensteiner S, Chetelat A, Martinoia E, Farmer EE. 2007*b*. A gain-of-function allele of TPC1 activates oxylipin biogenesis after leaf wounding in *Arabidopsis*. *The Plant Journal* **49,** 889–898.

Bonaventure G, Gfeller A, Rodriguez VM, Armand F, Farmer EE. 2007*a*. The fou2 gain-of-function allele and the wild-type allele of Two Pore Channel 1 contribute to different extents or by different mechanisms to defense gene expression in *Arabidopsis*. *Plant and Cell Physiology* **48,** 1775–1789.

Borjesson SI, Elinder F. 2011. An electrostatic potassium channel opener targeting the final voltage sensor transition. *Journal of General Physiology* **137,** 563–577.

Borjesson SI, Hammarstrom S, Elinder F. 2008. Lipoelectric modification of ion channel voltage gating by polyunsaturated fatty acids. *Biophysical Journal* **95,** 2242–2253.

Browse J. 2009. Jasmonate passes muster: a receptor and targets for the defense hormone. *Annual Review in Plant Biology* **60,** 183–205.

Browse J, Somerville C. 1991. Glycerolipid metabolism: biochemistry and regulation. *Annual Review in Plant Physiology and Plant Molecular Biology* **42,** 467–506.

Carpaneto A, Cantu AM, Busch H, Gambale F. 1997. Ion channels in the vacuoles of the seagrass *Posidonia oceanica*. *FEBS Letters* **412,** 236–240.

Carpaneto A, Cantu AM, Gambale F. 1999. Redox agents regulate ion channel activity in vacuoles from higher plant cells. *FEBS Letters* **442,** 129–132.

Carpaneto A, Cantu AM, Gambale F. 2001. Effects of cytoplasmic Mg^{2+} on slowly activating channels in isolated vacuoles of *Beta vulgaris*. *Planta* **213,** 457–468.

Dadacz-Narloch B, Beyhl D, Larisch C, Lopez-Sanjurjo EJ, Reski R, Kuchitsu K, Muller TD, Becker D, Schonknecht G, Hedrich R. 2011. A novel calcium binding site in the slow vacuolar cation channel TPC1 senses luminal calcium levels. *The Plant Cell* **23,** 2696–2707.

Gambale F, Cantu AM, Carpaneto A, Keller BU. 1993. Fast and slow activation of voltage-dependent ion channels in radish vacuoles. *Biophysical Journal* **65,** 1837–1843.

Gradogna A, Scholz-Starke J, Gutla PV, Carpaneto A. 2009. Fluorescence combined with excised patch: measuring calcium currents in plant cation channels. *The Plant Journal* **58,** 175–182.

Hedrich R, Neher E. 1987. Cytoplasmic calcium regulates voltage-dependent ion channels in plant vacuoles. *Nature* **329**, 833–835.

Hedrich R, Marten I. 2011. TPC1-SV channels gain shape. *Molecular Plant* **4,** 428–441.

Heinemann SH, Conti F. 1992. Nonstationary noise analysis and application to patch clamp recordings. *Methods in Enzymology* **207,** 131–148.

Ivashikina N, Hedrich R. 2005. K^+ currents through SV-type vacuolar channels are sensitive to elevated luminal sodium levels. *The Plant Journal* **41,** 606–614.

Lee Y, Lee HJ, Crain RC, Lee A, Korn SJ. 1994. Polyunsaturated fatty acids modulate stomatal aperture and two distinct K^+ channel currents in guard cells. *Cellular Signalling* **6,** 181–186.

Linden DJ, Routtenberg A. 1989. *cis*-Fatty acids, which activate protein kinase C, attenuate Na^+ and Ca^{2+} currents in mouse neuroblastoma cells . *Journal of Physiology* **419,** 95–119.

Meves H. 1994. Modulation of ion channels by arachidonic acid. *Progress in Neurobiology* **43,** 175–186.

Meves H. 2008. Arachidonic acid and ion channels: an update. *British Journal of Pharmacology* , **155,** 4–16.

Paganetto A, Carpaneto A, Gambale F. 2001. Ion transport and metal sensitivity of vacuolar channels from the roots of the aquatic plant *Eichhornia crassipes*. *Plant, Cell and Environment* **24,** 1329–1336.

Patel AJ, Lazdunski M, Honoré E. 2001. Lipid and mechano-gated 2P domain K^+ channels. *Current Opinion in Cell Biology* **13,** 422–428.

Pei ZM, Ward JM, Schroeder JI. 1999. Magnesium sensitizes slow vacuolar channels to physiological cytosolic calcium and inhibits fast vacuolar channels in fava bean guard cell vacuoles. *Plant Physiology* **121,** 977–986.

Peiter E, Maathuis FJ, Mills LN, Knight H, Pelloux J, Hetherington AM, Sanders D. 2005. The vacuolar Ca^{2+}-activated channel TPC1 regulates germination and stomatal movement. *Nature* **434,** 404–408.

Pérez V, Wherrett T, Shabala S, Muñiz J, Dobrovinskaya O, Pottosin II. 2008. Homeostatic control of slow vacuolar channels by luminal cations and evaluation of the channel-mediated tonoplast Ca^{2+} fluxes *in situ*. *Journal of Experimental Botany* **59,** 3845–3855.

Pottosin II, Dobrovinskaya OR, Muniz J. 2001. Conduction of monovalent and divalent cations in the slow vacuolar channel. *Journal of Membrane Biology* **181,** 55–65.

Pottosin II, Schonknecht G. 2007. Vacuolar calcium channels. *Journal of Experimental Botany* **58,** 1559–1569.

Ranf S, Wunnenberg P, Lee J, Becker D, Dunkel M, Hedrich R, Scheel D, Dietrich P. 2008. Loss of the vacuolar cation channel, AtTPC1, does not impair Ca^{2+} signals induced by abiotic and biotic stresses. *The Plant Journal* **53,** 287–299.

Rienmüller F, Beyhl D, Lautner S, Fromm J, Al-Rasheid KA, Ache P, Farmer EE, Marten I, Hedrich R. 2010. Guard cell-specific calcium sensitivity of high density and activity SV/TPC1 channels. *Plant and Cell Physiology* **51,** 1548–1554.

Schmidt D, MacKinnon R. 2008. Voltage-dependent K^+ channel gating and voltage sensor toxin sensitivity depend on the mechanical state of the lipid membrane. *Proceedings of the National Academy of Sciences*, *USA* **105,** 19276–19281.

Scholz-Starke J, Carpaneto A, Gambale F. 2006. On the interaction of neomycin with the slow vacuolar channel of *Arabidopsis thaliana*. *Journal of General Physiology* **127,** 329–340.

Scholz-Starke J, De Angeli A, Ferraretto C, Paluzzi S, Gambale F, Carpaneto A. 2004. Redox-dependent modulation of the carrot SV channel by cytosolic pH. *FEBS Letters* **576,** 449–454.

Scholz-Starke J, Naso A, Carpaneto A. 2005. A perspective on the slow vacuolar channel in vacuoles from higher plant cells. *Journal of Chemical Information and Modeling* **45,** 1502–1506.

Schulze C, Sticht H, Meyerhoff P, Dietrich P. 2011. Differential contribution of EF-hands to the Ca^{2+}-dependent activation in the plant two-pore channel TPC1. *The Plant Journal* **68,** 424–432.

Simard JR, Kamp F, Hamilton JA. 2008. Measuring the adsorption of fatty acids to phospholipid vesicles by multiple fluorescence probes. *Biophysical Journal* **94,** 4493–4503.

Singh SP, Zhou XR, Liu Q, Stymne S, Green AG. 2005. Metabolic engineering of new fatty acids in plants. *Current Opinion in Plant Biology* **8,** 197–203.

Yoshioka H, Sugie K, Park HJ, Maeda H, Tsuda N, Kawakita K, Doke N. 2001. Induction of plant gp91 phox homolog by fungal cell wall, arachidonic acid, and salicylic acid in potato. *Molecular Plant–Microbe Interactions* **14,** 725–736.